Electron Transit Time Enhancement In Photodetectors For High Speed Imaging

T. Kundu, R. K. Jarwal and D. Misra
Department of Electrical and Computer Engineering
New Jersey Institute of Technology, University Heights, Newark, NJ 07102-1982
Phone: +1-973-596-5680, Fax: +1-973-596-5680, E-mail: dmisra@njit.edu

Abstract

To operate at a fast frame rates with high sensitivity photoelectron transport in a photodetector under uniform illumination condition is investigated. The charge readout time of the photodetector with multi-implants is modeled with both diffusion equation and continuity equations were combined. A maximum effective diffusion length was assigned to each implanted regions after taking into account the fringing field drift due to multiple implants. It was assumed that the charge on each section is directly proportional to its area under uniform illumination. The total charge transport as a function of time is obtained by the superposition of charge contribution of all implanted regions. The design effects are also investigated. The model showed excellent match with experimental results.

I. Introduction

Sensitive imaging applications like optical wavefront measurements; explosion study and hypersonic gas turbulence require image acquisition at a frame rate much higher than 50/60 Hz, required for consumer applications. The sub-microsecond time resolution for these applications requires capturing images at the rate of 10^6 to 10^7 frames per second. Image sensors with ultra high frame rate (10^6 frames/sec or higher) were developed for studying rapid mechanical motion and transient phenomena [1, 2]. The imager with a large photodetector is required to obtain complete charge readout in much less than 1.0μs. . The optimal design for the detector with a transit time in sub-microsecond regime can be achieved if electrons are mostly drifted in the photodetector as shown in Fig. 1. A graded implantation for the photodiode can reduce the electron transit time. However, it is technologically extremely difficult to achieve such a profile. A multi-implant (graded) pinned-buried photodetector is, therefore, used to reduce the readout time. To achieve a high-speed detection, with essentially zero frame-to-frame lag, graded potential steps are created in the photodetector by variation of doping concentration of implants. To describe the photodetector charge readout time with multi-implants, a thermal diffusion model was developed [3]. According to this model the photodetector with *n* N-type detector implants is made up of *n* constant potential regions each with an effective L_{eff} separated by a step potential of about 0.5V. The effective photodetector charge readout time is estimated as the thermal diffusion decay time for the longest constant potential region plus an effective charge transfer between these regions. This model does not take into account the area or initial charge of individual implant and the effective diffusion lengths for near and far electrons. A charge transfer model for a 3-implant region was originally developed by our group [4]. The present paper is a more generalized thermal diffusion model which considers and *n*-implant case and takes into account the initial charge on each individual implant and the effective diffusion lengths of all electrons. Some design symmetry was also considered. The model compares the electron transit time in single implant, 3-implant and 7-implant photodiodes.

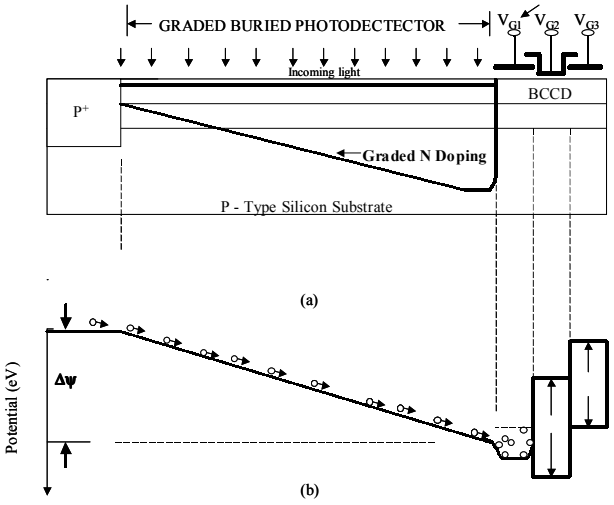

Fig. 1. A schematic of the graded photodide where electrons are mostly drifted to the collecting gate

II. THEORETICAL ANALYSIS

Thermal diffusion and fringing field drift govern the electron motion in a photodetector. Introducing the current density relation into continuity equation, and solving the partial differential equation the effect of thermal diffusion was studied. The solution is given by [5]:

$$Q(t) = \frac{8}{\pi^2} Q(0) e^{-\frac{t}{\tau}} \qquad \text{.....(1)}$$

where Q(t) is the charge at time t, Q(0) is the initial charge, L is the diffusion length, D_n is the diffusion coefficient, and τ is the diffusion time constant. The diffusion coefficient D_n is related to the electron mobility μ_n [6]. It can be seen from equation (1) that charge decreases exponentially with time from its initial value. The time constant of diffusion mechanism is inversely

proportional to D_n and directly proportional to the square of the diffusion length. For a high-speed photodetector L should be small and D_n should be large. A multi-implant photodiode, therefore, reduces the charge readout time.

The cross-sectional view of an *n*-N type implant pinned-buried photodetector is shown in Fig. 2(a). The implant concentration N1 is BCCD implant plus the first photodetector implant, N2 is N1 plus second photodetector implant, N3 is N2 plus the third photodetector implant and so on for Nn implant. These implants result in a graded potential profile along the photodetector as shown in Fig. 1(b). The potential profile divides the photodetector into *n*-sections where section-2 acts as a charge sink for section-1, section-3 acts as a charge sink for section-2 and so on. Finally, the potential well under the charge-collecting gate acts as a sink for the charge collected by the photodetector. The image acquisition cycle is the most important cycle of the imager, during this cycle the charge signal is detected by the photodetector, is transferred in series into the registers for detection of successive frames [3].

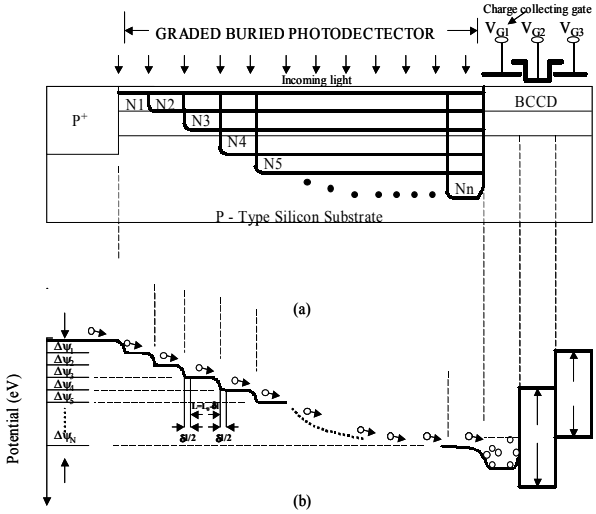

Fig.2 Cross sectional view of the *n*-N-type photodetector implant (a), graded potential profile and operation (b).

The total area of the photodiode is A and $A_1, A_2, A_3 \ldots A_n$ be the areas of implant regions. The implant area A_1 is divided into p number of small sections with an area of A_{1i} each. Similarly, implant areas $A_2, A_3 \ldots A_n$ are divided into $q,r \ldots m$ number of small sections with an area of A_{2j}, $A_{3k} \ldots A_{nm}$ for each small section. The total charge in the photodetector at any time t can be obtained by the superposition of charges in all small sections at time t. Mathematically it can be expressed as

where, $A_{1i} = i^{th}$ area of implant region A_1, $A_{2j} = j^{th}$ area of implant region A_2, $A_{3k} = k^{th}$ area of implant region A_3, and similarly $A_{nm} = m^{th}$ area of implant region A_n. D_{1n}, D_{2n}, D_{3n}, and D_{nn} are the electron diffusion coefficient of implant regions A_1, A_2, A_3, and A_n respectively. L_{1i}, L_{2j}, L_{3k} , and L_{nm} are the effective maximum diffusion lengths of electrons in i^{th}, j^{th}, k^{th} and m^{th} areas of implant regions A_1, A_2, A_3, and A_n respectively. The layout of 3-N type implant and 7-implant pinned-buried photodetectors are shown in Fig. 3(a) and Fig. 3(b) respectively. The individual areas for 3-implant case are well defined in Fig. 3(a) and the detailed outline of the individual areas in 7-implant case are specified in Fig. 3(b). The curves represent the cross-section. In Fig. 3(b) the symmetry in design reduces computation requirements for the model.

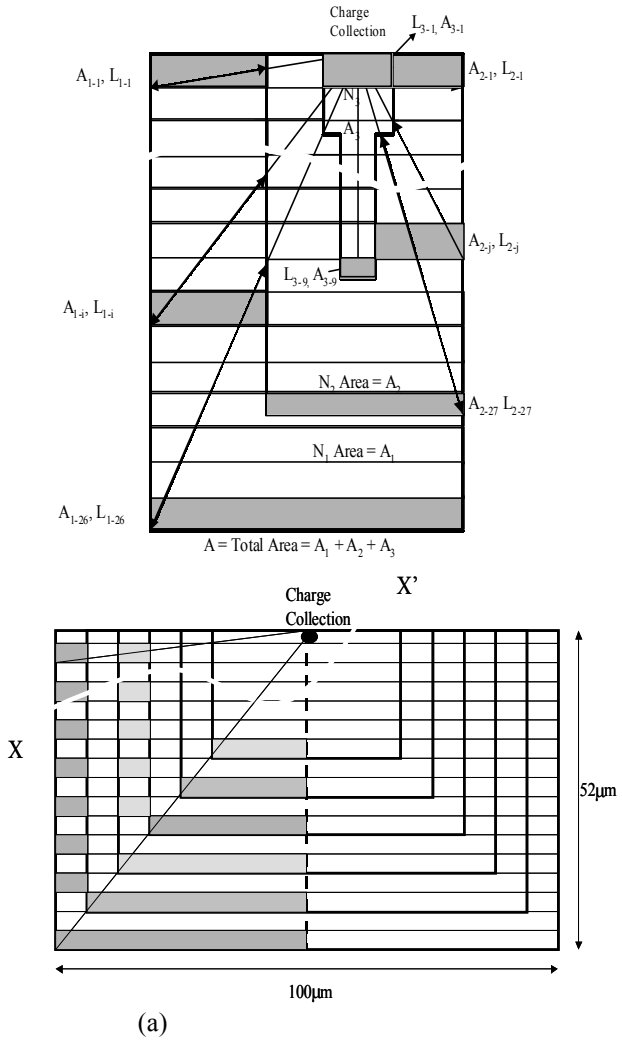

Fig. 3. Layout of a three N-type implant (a) and seven N-type implant (b) pinned-buried photodetectors.

$$Q(t) = \frac{8}{\pi^2}\frac{Q(0)}{A}\left[\sum_{i=1}^{p} A_{1i} e^{-\frac{\pi^2 D_{1n} t}{4L_{1i}^2}} + \sum_{j=1}^{q} A_{2j} e^{-\frac{\pi^2 D_{2n} t}{4L_{2j}^2}} + \sum_{k=1}^{r} A_{3k} e^{-\frac{\pi^2 D_{3n} t}{4L_{3k}^2}} \ldots\ldots \sum_{m=1}^{t} A_{nm} e^{-\frac{\pi^2 D_{nn} t}{4L_{nm}^2}}\right]$$

III. RESULTS AND DISCUSSION

Present model was used to compute the charge transfer for single N-type implant photodetector (70μm x 45μm) where N1 was 1.4×10^{17}cm^{-3}. The corresponding electron mobility and diffusion coefficient are 700 cm^2/V.sec and 18.145 cm^2/sec. For the 3-implant photodetector shown in Fig. 3(a) the doping concentrations are N1 ≈ 1.4×10^{17}cm^{-3}, N2 ≈ 2.6×10^{17}cm^{-3} and N3 ≈ 3.6×10^{17}cm^{-3}. The corresponding electron mobilities for these concentrations are $\mu_{1n} \approx 700$ cm^2/V.sec, $\mu_{2n} \approx 600$ cm^2/V.sec, $\mu_{3n} \approx 500$ cm^2/V.sec. These mobilities give three different diffusion coefficients $D_{1n} \approx 18.145$ cm^2/sec, $D_{2n} \approx 15.576$ cm^2/sec, and $D_{3n} \approx 12.994$ cm^2/sec for three implant regions. The effective maximum diffusion length of each section was computed by taking into account the fringing field drift [3]. In case of 7-implant photodetector (Fig. 3(b)) the doping concentrations were varied from N1 ≈ 1.4×10^{17}cm^{-3} to N7 ≈ 3.6×10^{17}cm^{-3} by equal increments. Therefore, the corresponding mobility values ranged from $\mu_{1n} \approx 700$ cm^2/V.sec to $\mu_{7n} \approx 500$ cm^2/V.sec and the diffusion coefficients were determined accordingly. Since the difference in doping concentration between two adjacent implants reduced, the fringing field also scaled down. These modifications need to be incorporated in the model for *n*-implant photodiodes.

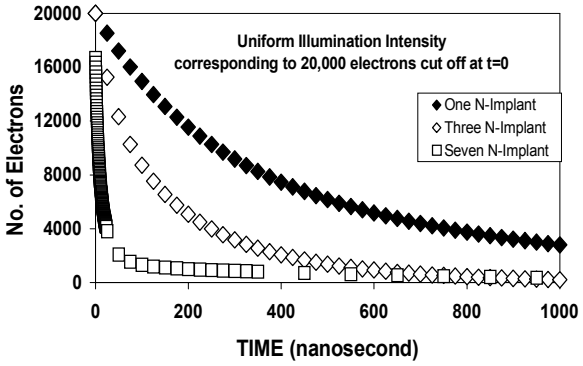

Fig. 4. Comparison between electron transfer characteristics for single N-type, three N-type and seven N-type implant photodetectors for uniform illumination corresponding to 20000 electrons is turned off at t=0.

Fig. 4 shows the comparison of electron transfer characteristics for single N-type implant, three N-type implant and seven N-type implant photodetectors after the uniform illumination intensity corresponding to 20,000 electrons is turned off at t=0. It can be seen that the charge readout time for three N-type photodetector is much smaller than one N-type implant photodetector. The number of electrons transferred from a small section to the collecting gate at time *t* depends on its initial number of electrons and maximum effective diffusion length or location from the collecting gate. Electrons are transferred from nearer sections to the collecting gate in a smaller time, whereas electrons from periphery of the photodetector take longer time. On the average, the electron transfer mechanism from implant region A_1 is slowest and fastest from implant region A_n. The total number of electrons in the photodetector is obtained by the superposition of the contribution of number of electrons from each small section. For 90% electron transfer the readout time for three-implant detector is about 500ns and for single implant detector readout time is more than 1000ns. For seven-implant case the readout further decreases to 50ns. This is a function of the doping profile distribution in the photodiode. By increasing *n* in an *n*-implant photodiode the transit time can be decreased further. When *n* is sufficiently high the stair case potential distribution will be a smooth profile and electron transport will take place mostly by drift due to the fringing field in the photodiode. A graded doping profile in the photodiode might reduce the number of masks and fabrication steps.

We have plotted the percentage of charge transfer as a function time for 7-implant photodiodes. Fig. 5 indicates the calculated intensity of the trailing image as a function of the time between the end of the light pulse and transfer of the photoelectrons in a 7-implant photodiode.

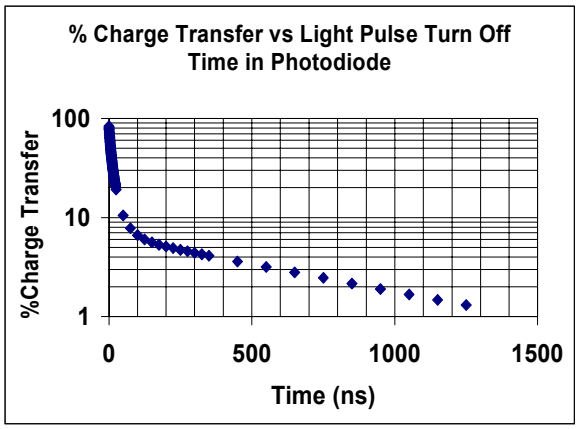

Fig. 5. Estimated charge transfer as a function of delay from light pulse to photodetector readout.

Charge readout comparison between the experimental results (1 MHz and 100 ns pulse) and the results obtained by using the present model is shown in Fig. 6. It can be seen that for 90% electron transfer the experimentally observed readout time is 500 ns and the readout time

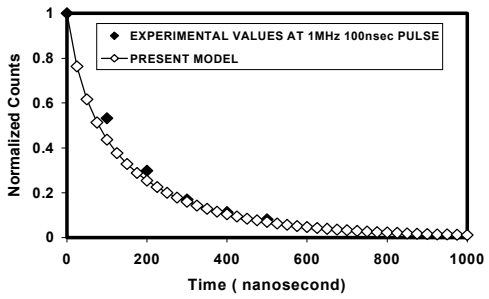

obtained by the present model is about 500ns.

Fig. 6. Comparison between the experimental charge readout values and charge readout values obtained by present model for a 3-implant photodiode.

IV. CONCLUSIONS

In conclusion, a thermal diffusion model has been developed for *n* N-type implant pinned buried photodetector. This model takes into account the initial charge of each implant and the effective length of the far and near electron. The model was used to estimate the charge transfer in 3-implant and 7-implant photodiodes. The model considers the fringing field effect at the interface of two adjacent implants. The results obtained by this model agree with the experimental values when compared in case of a 3-implant photodiode. By increasing the number of implants the transit time can be decreased further. However, many mask steps may be necessary but the staircase potential distribution will be a smooth graded profile and electron transport will take place mostly by drift due to the built in fringing field in the photodiode.

ACKNOWLEDGMENT

The authors wish to acknowledge Dr. J. L. Lowrance of Princeton Scientific Instruments, NJ for experimental data. The financial support from New Jersey Commission and NJ I-Tower project is acknowledged.

REFERENCES

[1] W. F. Kosonocky and J. L. Lowrance, " High Frame Rate CCD Imager", U.S. Patent 5 355 165, Oct. 11, 1994.

[2] W. Kosonocky et al., 360x360-Element Very High Frame-Rate Burst –Image Sensor", in Proc. 1996 IEEE Int. Solid State Circuits Conf., San Francisco, CA, pp. 182-183, 1996.

[3] G. Yang, "Design, Process, and Performance Simulation of a 360x360-Element Very High Frame-Rate Burst –Image Sensor," PhD Dissertation, New Jersey Institute of Technology, Newark, 1996.

[4] R.K. Jarwal, D. Misra and J.L. Lawrance, Charge Transfer in a Multi-Implant Pinned-Buried Photodetector," IEEE Trans. on Electron Devices, vol. 48, No.5, pp. 858-862, May 2001.

[5] J. E. Carnes, W. F. Kosonocky, and E. G. Ramberg " Free Charge Transfer in Charge Coupled Devices" IEEE Trans. Electron Devices, vol. ED-19, pp. 798-802, 1972.

[6] S. M. Sze, Semiconductor Devices Physics and Technology, John Wiley and Sons, New York, NY, 1985(ISBN-0471-87424-8).